ADVANCED ENGINEERING MATERIALS
www.aem-journal.com

Thermal and Electrical Conductivity of Copper-Graphene Heterosystem: An Effect of Strain and Thickness

Aiswarya Samal, Anoop Kumar Kushwaha, Debashish Das, Mihir Ranjan Sahoo, Nicholas A. Lanzillo, and Saroj Kumar Nayak*

Copper-graphene (Cu/Gr) composite carries high thermal (κ) and electrical (σ) conductivities compared with pristine copper film/surface. For further improvement, strain is applied (compressive and tensile) and the thickness is changed (of both copper and graphene). It is observed that electronic thermal conductivity (κ_e) and σ enhance from 320.72 to 869.765 W mK^{-1} and 5.28 × 10^7 to 23.01 × 10^7 S m^{-1}, respectively, by applying 0.20% compressive strain. With the increase in copper thickness (three to seven layers) in Cu(111)/single-layer-graphene (SLG) heterosystem, κ_e increases from 320.72 to 571.81 W mK^{-1} while electrical resistivity ($\rho \propto (1/\sigma)$) decreases from 0.189 × 10^{-7} to 0.117 × 10^{-7} Ωm. Furthermore, with the increase in graphene thickness (one to four layers) in seven-layer Cu(111)/multilayer-graphene (MLG) heterosystem, κ_e enhances upto 126% while ρ decreases upto 70% compared with the three-layer Cu(111)/SLG. A large available state near Fermi level (of Cu/Gr heterosystem) offers the conduction of more electrons from valence to conduction bands. With increasing copper/graphene thickness, this state is further broadened and provides an enhancement in conduction electrons. The electron localization function decreases with increasing thickness at the copper-graphene junction, suggesting electrons are delocalized at the junction, resulting in an increase of free electrons that enhance κ_e and σ. Herein, it is useful in advancing the thermal management of electronic chips and in applying hybrid copper-graphene interconnects.

1. Introduction

As electronic devices approach the nanoscale dimension, the power density of integrated circuits increases rapidly, creating a serious problem in the thermal management system. To deal with such issues, graphene (Gr) is reported as an efficient candidate for next-generation low-power electronic devices at the nanoscale level.[1] Graphene, a two-dimensional (2D) crystalline allotrope of carbon, has one atomic layer thickness and a honeycomb lattice structure. Graphene possesses extraordinary properties due to its high carrier mobility at room temperature, ultrahigh thermal, and electrical conductance.[2,3] The high thermal (TC; κ) and electrical (EC; σ) conductivities of graphene make it a suitable material for thermal management. TC consists of electronic thermal conductivity (ETC; κ_e) and phonon thermal conductivity (PTC; κ_p) which provide the transport properties of the electron and phonon, respectively. The TC and EC of graphene are well-studied properties. For example, Baladin et al.[1] observed the TC of single-layer graphene (SLG) in the range of 4800–5300 W mK^{-1} using the confocal micro-Raman spectroscopy method, whereas Ghosh et al.[4] found it in the range of 3080–5150 W mK^{-1}. The TC of graphene is found to be in the range of 3200–4000 W mK^{-1} using the density functional theory and Boltzmann transport equation (DFT-BTE) method.[5] Kim et al.[6] observed that κ_e of graphene is nearly 10% of the κ_p due to its semimetal nature. As a result, κ_p dominates κ_e in graphene. In contrast to graphene, κ_e possesses a comparatively higher value than κ_p on the metal surface.[7,8] For example, κ_p of copper and aluminum is reported as 16.9 and 5.8 W mK^{-1}, respectively, which are negligible compared to κ_e of copper (501.00 W mK^{-1}) and aluminum (220.00 W mK^{-1}).[7,9] However, Tong et al.[10] have found that κ_p (in the range of 2–18 W mK^{-1}) accounts for 1–40% of the total TC in transition metals. This represents that κ_p is a non-negligible component of TC due to high phonon group velocities. Wang et al.[7] studied phonon–phonon (ph-ph) and electron–phonon (el-ph) scattering in metals and found that el-ph scattering is negligible in Cu, Ag, Au, and Al, while significant in Pt and Ni at room temperature.

Copper has high TC (401.00 W mK^{-1}) and EC (5.96 × 10^7 S m^{-1}), good corrosion resistance properties, and an environmentally friendly nature.[11] Therefore, it is widely used in integrated circuits, electrical conductors, radiators, etc.[11,12] In contrast, electromigration, low scalability, high resistivity, poor mechanical properties, and other performance hindrances restrict the application of copper-based interconnect.[13] Graphene-reinforced metal composites show superior performance to pristine metal in terms of mechanical strength, EC and TC, and weight.[14–16] The metal contacts with graphene

A. Samal, A. K. Kushwaha, D. Das, M. R. Sahoo, S. K. Nayak
School of Basic Sciences
Indian Institute of Technology Bhubaneswar
Khordha, Odisha 752050, India
E-mail: nayaks@iitbbs.ac.in

N. A. Lanzillo
IBM Research
257 Fuller Road, Albany, NY 12203, USA

The ORCID identification number(s) for the author(s) of this article can be found under https://doi.org/10.1002/adem.202201192.

DOI: 10.1002/adem.202201192

enhance the TC of heterogeneous films.[13,17,18] This provides a noble way to design a heat dissipation component in electronic devices.[19] For example, Goli et al.[13] observed a larger TC of graphene–copper–graphene heterogeneous films compared to pristine and annealed copper films. Similar results are observed in Cu/Gr layers for both cross-plane and in-plane directions.[20] Further, the copper-matrix nanocomposite highly aligned with graphene platelets enhances TC up to 140%.[21] Apart from Cu/Gr heterosystems, the interfacial thermal transmission and resistance of various metal/graphene (Cu/Gr, Pd/Gr, Ni/Gr, and Au/Gr) heterosystems have been investigated.[19] The interfacial thermal resistances of the Ni/Gr, Cu/Gr, Au/Gr, and Pd/Gr heterosystems are reported as 3.90×10^{-8}, 1.18×10^{-8}, 1.72×10^{-8}, and 3.35×10^{-8} $Km^2 W^{-1}$, respectively. The study of TC and EC is crucial for replacing aluminum/silicon-based CMOS (complementary metal–oxide semiconductor) by the Cu/Gr heterosystem. For Cu/Gr nano-interconnects, the conductivity is comparatively larger than that of pristine copper due to having a more available density of states (DOS) at the Fermi level for graphene on copper system.[22] Mehta et al.[18] observed a drastic enhancement in both TC and EC through the deposition of graphene around copper nanowires.

The TC and EC of graphene and metals are highly affected by applying strain, which has already been studied theoretically and experimentally.[23] Ma et al.[24] observed that applying strain reduces the TC of graphene due to increased Umklapp scattering. Furthermore, strain applied to graphene downshifts the frequencies of the optical phonon modes. Using nonequilibrium molecular dynamics (NEMD), Guo et al.[5] and Wei et al.[23] investigated the strain effect on graphene nanoribbon and found that TC was significantly reduced due to phonon softening. Bazrafshan et al.[25] studied pristine and amorphous graphene by applying tensile strain and observed that TC decreased as strain increased up to 12%. In the case of metal, Lee et al.[26] applied tensile strain (0.25%) to an aluminum film and observed a lower TC and higher electrical resistivity (ER; ρ) values. Even when the nature of the strain changes (i.e., from compressive to tensile), TC reduces, as seen in the case of silicon.[27] The thickeness variation affects the TC, as observed in the case of copper.[28] An enhancement in the TC is observed by varying the thickness from single-layer graphene (SLG) to multilayer graphene (MLG) in the copper-graphene nanocomposite.[17]

In recent years, various properties of the Cu/Gr heterosystem have been studied with both experiment and theory.[11,13,16,18,20,29,30] All studies suggest that the EC and TC of Cu/Gr are higher compared to those of pristine copper. By changing the composition percentage ratio, the TC and EC increase only up to a certain value. To further enhance them, we have engineered the surface and interface of the Cu/Gr heterosystem. Here, we have used two methods: 1) applying tensile and compressive strain; and 2) varying the thickness of graphene and copper. Due to the negligible κ_p value, the κ_e contributed primarily to TC in the high-temperature region (above the Debye temperature (θ_D) as per Wiedemann–Franz law ($(\kappa_e/\sigma) = LT$, where L is the Lorentz factor and T is the absolute temperature).[31] The electrical energy carriers (electrons) and thermal energy carriers (electrons and phonons) are scattered by deformation mechanisms. Therefore, with the prior concept that thermal and electrical transportation is influenced by mechanical strain, we have studied the effect of strain on the Cu/Gr heterosystem. In metals, electrons carry both heat and electricity, and they are scattered by dislocations and grain boundaries.[26]

In short, through first-principles DFT and density functional perturbation theory (DFPT) in conjunction with the Boltzman transport equation (BTE),[8] we have investigated the transport properties of bulk copper, Cu(111) surfaces, and the Cu/Gr heterosystem by applying both tensile (positive) and compressive (negative) strain up to ±0.5%. Beyond that limit, the structures are distorted.[26] The ETC and EC have been derived from the lowest order variational solution of BTE.[8,32] Further, we have studied binding energy, formation energy, TC, and EC through variation of copper (from three to seven layers) and graphene (from one to four layers) layer thickness in the Cu/Gr heterostructure. The origin of the large TC and EC has been probed through analysis of electronic band structure, DOS, charge density, and electron localization function (ELF), which are discussed thoroughly in the results and discussion.

2. Computational Methodology

All the geometrical relaxation has been carried out using DFT-based Quantum Espresso code. The projector-augmented wave (PAW) method[33] has been included in the Perdew, Burke, and Ernzerhof (PBE)[34] exchange-correlation potential under the generalized gradient approximation (GGA). The plane-wave expansion energy cutoff is fixed at 60Ry. Marzari-vanderbilt first-order spreading is used with a smearing width of 0.01 eV and a $12 \times 12 \times 1$ k-point mesh for geometry optimization. During relaxation, the self-consistency criteria are set to 1×10^{-8} eV. A vacuum of 20 Å has been introduced in the z-direction to avoid the interaction between the surfaces due to periodic boundary conditions. To calculate PTC at a finite temperature, first we obtained an atomic structure (with minimum energy) at zero temperature; consequently, this structure is used for high-temperature calculations.[9] This is performed using PHONO3PY, which is incorporated into Quantum Espresso.[35,36] To obtain atomic forces, the total energies were minimized until the energy convergences became less than 1×10^{-9} eV. For the TC calculation, $2 \times 2 \times 2$ supercell is used for bulk copper, while a $2 \times 2 \times 1$ supercell is selected for the Cu(111) surface and the Cu(111)/Gr heterosystem, respectively. Here, we have used a finite atomic displacement of 0.06 Å for the supercell approach to calculate second-order and third-order force constants. For sampling third- and second-order force constants, we used $2 \times 2 \times 2$ and $3 \times 3 \times 1$ k-point meshes for bulk copper and Cu(111) surface calculations, respectively. The κ_e and σ are computed using DFT-based ABINIT code.[7] The electron–phonon (el-ph) matrix element for bulk copper is calculated on a q-grid of $4 \times 4 \times 4$ q-points and a k-grid of $36 \times 36 \times 36$ k-points. The el-ph matrix element of the Cu(111) surface and Cu/Gr is calculated on a $4 \times 4 \times 1$ q-grid and a $20 \times 20 \times 1$ k-grid. The plane wave energy cutoff for all the calculations is fixed at 20.0 Hartree. The total-energy frozen-phonon approach has been used to obtain the phonon frequencies, phonon eigenvectors, and electron–phonon interaction.[32,37,38] To determine the coupling strength of λ, a large number of phonon wave vectors are sampled in the Brillouin zone. A separate frozen phonon

calculation is required for each wave vector. We have calculated the electrical resistivity and TC by using a lowest order variational approximation of the Boltzmann transport equation (BTE).[32,39]

To see the effect of exchange-correlation potentials on the results (e.g., TC and EC), we have studied the charge density (shown in Figure S1 of the Supporting Information) of the Cu(111)/graphene unit cell using both PBE and HSE06 (hybrid functional). We did not observe any significant charge density delocalization through the PBE. The charge density, calculated with both PBE and HSE06 functional, is identical and does not show any deformation on C (in graphene), Cu (in the surface), or on their interfacial region. Since both functions carry an identical charge distribution on the interface, their interfacial properties will not change significantly. Thus, introducing a HSE06 will not alter the nature of the results. A similar conclusion has been reached for hexagonal boron arsenide, where TC has been studied by applying strain.[40] The study found that the difference between the electronic band structure calculated through PBE and HSE06 is very small, and their variation with strain shows the same trend with both functions.[40] The correlation energy of HSE06 is the same as PBE; however, the differences arise due to the introduction of a semilocal behavior by mixing the exchange from Hartree–Fock, which improves the accuracy. Although HSE06 can provide a bandgap value with higher accuracy compared to GGA-PBE, it is computationally very expensive. PBE has been used in previous studies based on phonon analysis, TC, and EC of 2D materials because it maintains accuracy close to HSE06.[40] Thus, the results will be insensitive to the functional (HSE06 or PBE).

3. Results and Discussion

3.1. Geometrical Structures of Copper-Graphene (Cu/Gr) Interfaces

The lattice constants of 2D materials must match to form heterostructures. The in-plane lattice constant of graphene (2.46 Å) shows good compatibility with the Cu(111) surface (2.55 Å). There are three configurations for placing carbon atoms (of graphene) on the Cu(111) surface, as shown in Figure S2 (Supporting Information). The top-fcc position (**Figure 1**A) has the lowest energy and is the most stable configuration.[29,30,41] As a result, the Cu/Gr heterostructure is formed by placing a 1×1 unit cell of graphene on the top-fcc (A1) position of a Cu(111) surface (of 1×1 unit cell).[11,29,30,42,43] In this arrangement, one carbon atom of the graphene primitive cell lies on the first layer of Cu(111) surface, and the second carbon atom lies on the third layer of Cu(111) surface. The Cu/Gr heterostructure unit cell consists of three Cu-atoms (of Cu(111)) and two C-atoms (of SLG). The effect of applied strain has been studied on a three-layer Cu(111)/SLG heterostructure. To study the effect of thickness, we have increased the layers of Cu(111) and graphene up to seven and four layers, respectively, as shown in Figure 1 and S3 and S4 (in Supporting Information). All the structures are

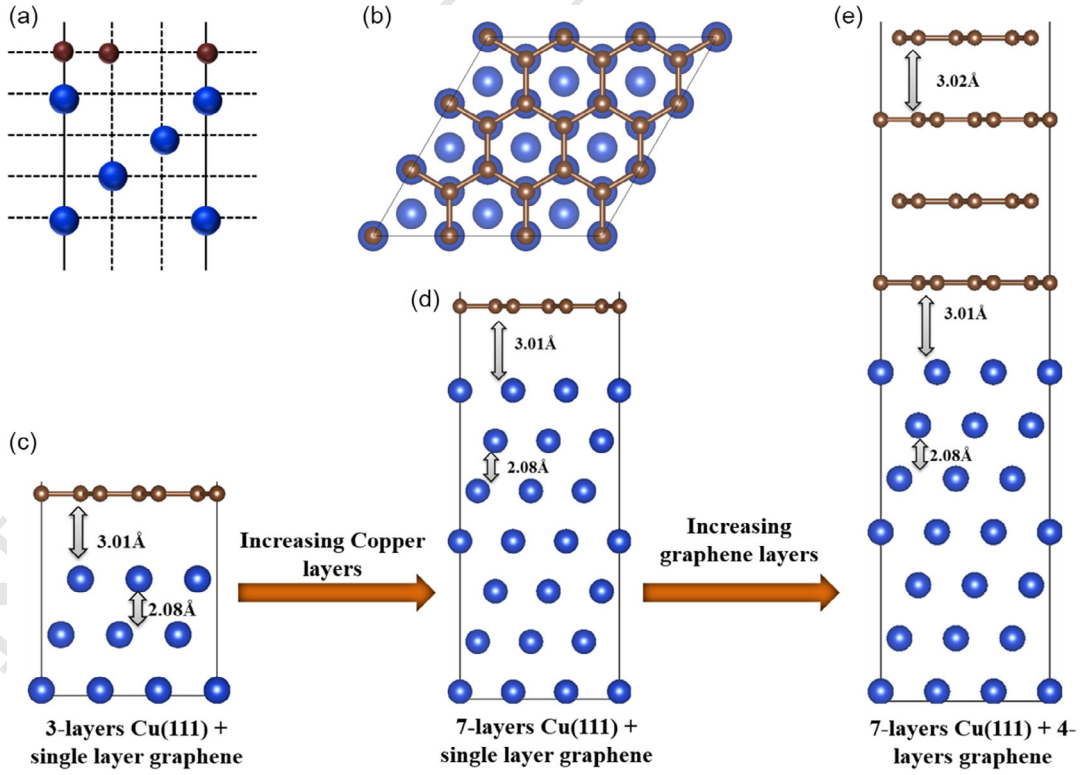

Figure 1. Schematic diagrams of A) the top-fcc arrangement of the Cu(111)/graphene heterosystem, B) the top view of the Cu(111)/graphene heterosystem, C) three-layer Cu(111) surface with single layer graphene (SLG), D) seven-layer Cu(111) surface with SLG, E) seven-layer Cu(111) surface with four-layer graphene. The blue and brown spheres indicate the Cu- and C-atoms, respectively.

relaxed with the aforementioned methods (see Computational Methodology section). Graphene's hexagonal closed pack lattice is similar to the triangular lattice of metals having fcc(111) and hcp(0001).[11,29,30,42–44] The distance between Cu(111) and SLG in all Cu/Gr heterosystems (with varying thicknesses) is ≈3.00 Å, which shows a good agreement with previous results.[42,44] The separation between the graphene layers and the Cu(111) layers is ≈3.02 and ≈2.08 Å, respectively.

3.2. Tensile and Compressive Strain Effect

Tensile and compressive strains are applied to bulk copper, the Cu(111) surface, and the Cu/Gr heterostructure to investigate their effects on TC and EC. In the bulk copper, strain was applied in the *X*-, *Y*-, and *Z*-directions, but only in the *X*- and *Y*-directions in the Cu(111) surface and Cu/Gr heterostructures. Under periodic boundary conditions, the strain has been applied by varying the lattice constant of the unit cell according to the actual lattice constant value. The percentage of applied strain (δ) is calculated using Equation (1)

Q4

$$\delta = \frac{a - a_0}{a_0} \times 100 \tag{1}$$

where a and a_0 are the lattice constants of the material with and without strain, respectively.

On the bulk copper, we applied compressive (negative) and tensile (positive) strains ranging from −0.5% to 0.5%. Figure S5 (Supporting Information) shows that both κ_e and σ decrease with increasing tensile strain, while both are enhanced by applying compressive strain. The lattice constant and κ_p of bulk copper with various applied strains have been listed in Table S1 and S2 (in Supporting Information). There is a very small contribution of κ_p (≈10 W m K^{-1}) in TC, which is enhanced only up to ≈20 W mK^{-1} through applying strains. Thus, κ_e(= 520.247 W mK^{-1}) plays the dominant role in TC over κ_p. Therefore, phonon transport in copper can be ignored due to its very small contribution. The σ of bulk copper is observed as 7.66×10^7 S m^{-1}. The electron transport in the metals is limited by electron–phonon (el-ph) scattering in high-temperature regions. The ab initio linear response method is used to find the el-ph coupling constant (λ).[32,39] The λ of copper is 0.08, which is in good agreement with the previously reported value of 0.14.[32] With applied tensile strain, λ (from 0.082 to 0.094) increases while κ_e (from 522.04 to 460.19 W mK^{-1}) and σ (from 7.701×10^7 to 6.726×10^7 S m^{-1}) decreases (see Figure S5 in the Supporting Information). On the other hand, compressive strain reduces the λ (from 0.082 to 0.078) and enhances the κ_e (from 522.04 to 550.00 W mK^{-1}) and σ (7.701×10^7–8.153×10^7 S m^{-1}). As a result, el-ph coupling acts as a resistance for κ_e and σ in the bulk copper. In short, the compressive strain reduces the λ value while the tensile strain increases it. This is consistent with a previous study in which λ of metal was reduced by applying pressure.[39] Similarly to other metals, the el-ph scattering contribution in κ_e and σ is dominated by electron–electron and electron impurity scatterings in bulk copper.[39]

In the three-layer Cu(111) surface, the numerical values of κ_e and σ are 211.574 W mK^{-1} and 3.07×10^7 S m^{-1}, respectively (see Figure S6 in the supporting information). These are smaller than bulk copper. The primary reason for such changes is associated with the scattering of the electron from the top and bottom of the film boundaries (where the film thickness is comparable to the mean free path of the electron).[28] It has been experimentally observed that the grain size in copper decreases with decreasing film thickness.[28,45] Figure S6 (Supporting Information) shows how the compressive strain (from 0.05% to 0.40%) affects σ and κ_e of Cu(111) surface. The κ_e (211.57 W mK^{-1}) of Cu(111) agrees well with the previous result.[46] Both σ and κ_e increased until 0.15% and then rapidly decreased. On the other hand, λ decreases with strain until 0.15%, after which it drastically increases (see Figure S7 in the Supporting Information). Applying a compressive strain to Cu(111) compresses the lattice, making the effective "springs" between atoms more rigid, resulting in higher frequency phonons. Higher-frequency phonons are less effective at scattering electrons and provide a weaker electron–phonon coupling for compressed copper in comparison to its equilibrium (without strain) configurations. Any reduction in electron–phonon coupling will be reflected in a reduction in the electrical resistivity.[47] In other words, as copper's electron–phonon coupling (λ) decreases, so does its electrical resistivity (/conductivity) decreases (/increases). In our case, applying 0.15% strain reduces λ, and thus electrical resistivity ($\rho = 1/\sigma$) decreases. According to the Wiedemann–Frantz law, the electrical conductivity (σ) is proportional to thermal conductivity (κ); thereby increasing σ increases κ. Thus, λ (0.36–0.17) decreases whereas σ (3.07×107–3.78×107 S m^{-1}) and κ_e (211.57–257.64 W mK^{-1}) increase by applying strain upto 0.15%. Giri et al.[39] observed a similar result where decreasing metal's electron–phonon coupling significantly increases electrical and electronic thermal conductivities. When the compressive strain exceeds 0.15%, the value of λ increases, causing the σ and κ to decrease. However, the transition between increased/decreased electrical/thermal conductivity and the electron–phonon coupling constant, around 0.15% compressive strain, remains an area for further research.

In the SLG, the κ_p, and κ_e are observed as 3000.378 and 194.951 W mK^{-1}, respectively. These values are in good agreement with earlier reports.[6] In SLG, the κ_p dominates over κ_e, which is in contrast to that of copper. SLG experiences 3.85% tensile strain when its 1 × 1 unit cell is placed in the top-fcc position of Cu(111). If we apply 3.85% tensile strain on the SLG, the κ_p and κ_e reduce up to 725.987 (from 3000.378 to 2274.391 W mK^{-1}) and 31.486 W mK^{-1} (from 195.000 to 163.154 W mK^{-1}), respectively, as shown in Figure S8 (Supporting Information). This result is supported by the experimental observation where Li et al.[14] found a reduced TC by applying compressive and tensile strain on graphene. Apart from SLG, the strain effect on multilayer graphene (MLG) has also been extensively studied.[6,48–50] The TC of pristine/modified graphene varies in the range of 2600–5300 W mK^{-1}, which is much higher than other materials.[50–53] The κ_e (= 300 W mK^{-1}) observed in the doped SLG was only ≈10% of the κ_p.[6] Mathematically, κ_p of a semiconductor is expressed by Equation (2) as follows[27]

$$k_p = \frac{1}{3}\sum_{k,p} C_{k,p}\, v_{k,p} \lambda_{k,p} \tag{2}$$

where C, ν, and λ are specific heat, average group velocity, and mean free path of phonons, respectively. With the introduction of compressive strain, the phonon group velocity of acoustic phonons increases due to the upward shift of the phonon dispersion curve.[27] Thus, TC increases with increasing phonon-specific heat. A contrast in behavior is found by applying tensile strain, where TC decreases with increasing tensile strain.

Figure 2a,b depicts the temperature dependence nature of κ_e and σ of the Cu(111) surface and the Cu(111)/Gr heterosystem, respectively. At the room temperature, κ_e and σ of the Cu(111)/Gr heterosystem are found to be 320.73 W mK^{-1} and 5.28×10^7 S m^{-1}, respectively, which are higher than those of the Cu(111) surface ($\kappa_e = 211.57$ W mK^{-1}; $\sigma = 3.07 \times 10^7$ S m^{-1}). Thus, κ_e and σ of the Cu/Gr heterosystem enhance by up to 52% and 70%, respectively, when compared to Cu(111) surface. The qualitative enhancement is consistent with the previous reports.[13,46] For example, Goli et al.[13] found that the TC of copper (9 µm thick) and copper-graphene composite were ≈285 and ≈370 W mK^{-1}, respectively. Furthermore, Zheng et al.[46] determined that copper substrate and nitrogen-doped graphene-copper composite have TCs in the 370–400 and 530–560 W mK^{-1} ranges, respectively. Thus, the copper-graphene composite has a greater TC value than pristine copper in both experimental observations. In other words, graphene deposition on copper enhances TC significantly, which is qualitatively consistent with our findings. Here, the exact experimental thickness may not be directly mimicked using our method due to the computationally demanding task. However, the trend of EC and TC versus thickness, both from theory and experiment, indeed agrees, suggesting the essence of the physics is captured in our model calculation. The electrons and phonons are dominant as heat carriers in copper and graphene, respectively. The κ_p of Cu(111) surface (8.45 W mK^{-1}) and Cu(111)/Gr heterosystem (8.00 W mK^{-1}) were found to be much lower than κ_e of Cu(111) surface (211 W mK^{-1}) and Cu(111)/Gr heterosystem (163 W mK^{-1}). Thus, due to the small contribution of κ_p compared to κ_e, we have emphasized only κ_e part of the Cu(111) surface and Cu/Gr heterostructure. The increase in temperature up to 1000 K had no significant effect on κ_e, while σ drastically decreases with increasing temperature and becomes saturated after a certain temperature. We studied the effect of compressive strain (from 0.05% to 0.4%) on κ_e and σ of the Cu/Gr heterosystem. Figure 2c,d shows that by applying compressive strain up to 0.2%, both κ_e and σ increase up to ≈869.765 W mK^{-1} and ≈23.01×10^7 S m^{-1}, respectively. Both are reduced and saturate at ≈787 W mK^{-1} and ≈21×10^7 S m^{-1} beyond 0.2% compressive strain.

Thus, applying 0.2% compressive strain to the Cu(111)/graphene heterostructure increased κ_e and σ up to 549.04 W mK^{-1}

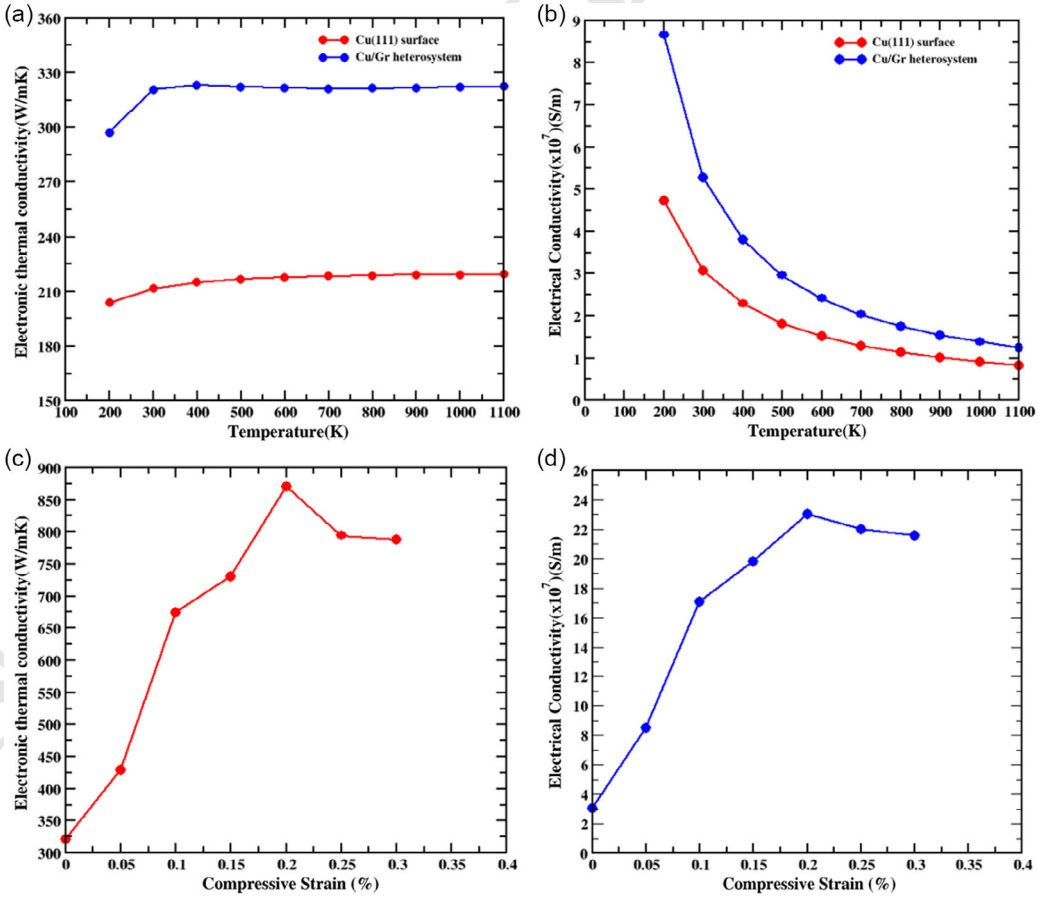

Figure 2. a) Electronic thermal conductivity (κ_e). b) Electrical conductivity (σ) of Cu(111) surface and Cu/Gr heterosystem with increasing temperature. Compressive strain effect on c) κ_e d) σ of Cu/Gr heterosystem at room temperature.

(from 320.72 to 869.76 W mK^{-1}) and 17.73×10^7 S m^{-1} (from 5.28×10^7 to 23.01×10^7 S m^{-1}), respectively. In the Cu(111)/graphene system, graphene already has a 3.85% tensile strain, whereas Cu(111) has no initial strain. On applying a compressive strain (e.g., 0.2%) to the Cu(111)/graphene system, the graphene surface lattice is suppressed and tends toward an equilibrium (without strain) configuration, while Cu(111) feels exactly the same (0.2%) compressive strain. If we apply 0.2% compressive strain on graphene (which is already under 3.85% tensile strain), the κ_e and κ_p increase up to ≈17 (from ≈163 to ≈180 W mK^{-1}) and ≈325 W mK^{-1} (from ≈2275 to ≈2600 W mK^{-1}), as shown in Figure S8 (Supporting Information). Thus, by applying 0.2% strain to graphene, total TC increases up to ≈ 342 W mK^{-1}. This enhancement by applying compressive strain is consistent with a previous report in which TC increased with strain application.[27] Similarly, when a 0.2% compressive strain is applied to Cu(111), κ_e increases by up to ≈50 W mK^{-1}, as shown in Figure S6 (Supporting Information). Thus, combined graphene (≈350 W mK^{-1}) and Cu(111) (≈50 W mK^{-1}) contribute ≈400 W mK^{-1} in TC of a total ≈550 W mK^{-1} which is raised by applying ≈0.2% compressive strain to the Cu(111)/graphene heterostructure. The remaining TC is caused by electron–phonon scattering because λ reduces up to ≈0.18 by applying 0.2% compressive strain. This means that electron–phonon interaction is suppressed at 0.2% compressive strain. The copper's electrical resistivity (/conductivity) decreases (/increases) due to reducing electron–phonon coupling.[39,47] According to Wiedemann–Frantz law, EC is proportional to TC; thus, increasing EC enhances TC.[31] A similar result was observed by Giri et al.,[39] who found that a small reduction in the electron–phonon coupling factor of metals enhanced electrical and electronic thermal conductivities largely. This is consistent with the λ of Cu(111)/graphene heterostructure, as shown in **Figure 3**. Here, at ≈0.2% compressive strain, λ has the lowest value due to suppressed electron–phonon scattering, resulting in an enhancement in TC.

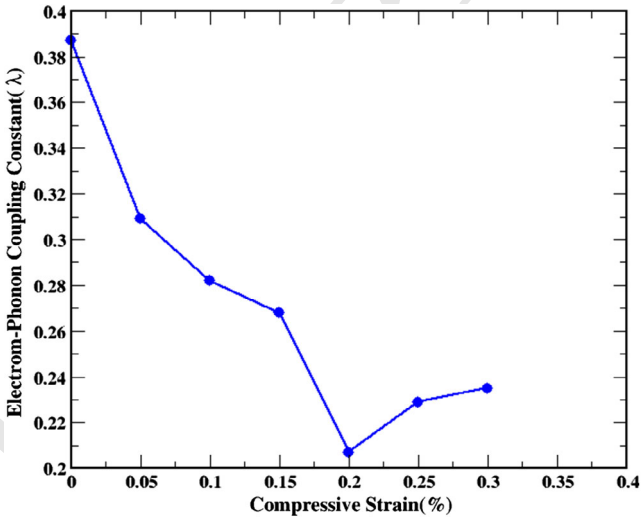

Figure 3. Effect of compressive strain on the el-ph coupling constant (λ) of Cu/Gr heterosystem.

The enhancement in the TC by applying 0.2% strain is primarily contributed by phonon (of graphene) and electron–phonon scattering. Therefore, there will be no significant change in the geometrical and electronic structure of the Cu(111)/graphene heterostructure by applying a very small strain. This is consistent with a negligible change in the C—C bond (of graphene; 0.004 Å), Cu—Cu bond (on the copper surface; 0.005 Å), distance between copper layers (0.009 Å), and copper–graphene interlayer distance (≈0.1 Å) by applying 0.2% compressive strain (see Figure S9 in Supporting Information). Also, the DOS of the Cu(111)/graphene heterostructure does not show a significant change under the 0.2% compressive strain, as shown in Figure S10 (Supporting Information).

3.3. Thickness Effect

To study the effect of thickness on κ_e and ρ of the Cu/Gr heterosystem, we have used two methods: 1) increasing copper thickness by adding three to seven layers of Cu(111); and 2) increasing graphene thickness by adding one to four graphene layers. The geometrical structures of Cu(111)/SLG and Cu(111)/MLG heterostructures are discussed in Section 3.1 and shown in Figure 1 and S3 and S4 (in the Supporting Information). **Figure 4**a shows that copper's κ_e increases up to 233.633 W mK^{-1} (from 211.574 to 445.207 W mK^{-1}) by adding copper layers (from three to seven) at room temperature. Similarly, Figure 4b demonstrates that κ_e of the Cu(111)/SLG heterosystem increases up to 251.084 W mK^{-1} (from 320.726 to 571.810 W mK^{-1}) by increasing the copper thickness (from three to seven layers) in the heterosystem. In contrast, ρ decreases from 0.32×10^{-7} to 0.15×10^{-7} Ωm (in copper; Figure 4c) and from 0.189×10^{-7} to 0.117×10^{-7} Ωm (in the Cu(111)/SLG hetersystem; Figure 4d) by adding copper layers at room temperature. Thus, increasing the thickness of the Cu(111), κ_e increases, while ρ decreases up to the seven-layer thickness. At the seven-layer thickness of Cu(111), both (i.e., κ_e and ρ) are saturated, and adding more layers has no significant effect on these values.

The Fuchs–Sondheimers (FS) surface scattering and Mayadas–Shatzkes (MS) grain boundary scattering models are generally used to investigate the thickness-dependent resistivity of metal films (e.g., copper, silver, and aluminum). These models show that film thickness and electrical resistivity (ρ) have an inverse relationship. Zhang et al.[11] found that as film thickness (5–100 nm) increases, electrical resistivity decreases rapidly up to a critical thickness and then gradually decreases. The thickness dependence on resistivity is directly associated with the electron mean free path (EMFP) of materials. The thickness/size effect of resistivity is reduced when the material has a smaller EMFP. Thermal conductivity (κ) is also strongly dependent on the thickness of the copper surface. Nath et al.[28] investigated thickness-dependent variation of κ for copper films with thicknesses ranging from 400 to 8000 Å. According to their findings, the thermal conductivity increases with film thickness due to scattering of the conduction electrons from the film surface, the scattering of lattice impurities, and frozen-in structural defects in the film. Furthermore, there is a distinction between surface and bulk conduction in copper. For very thin films,

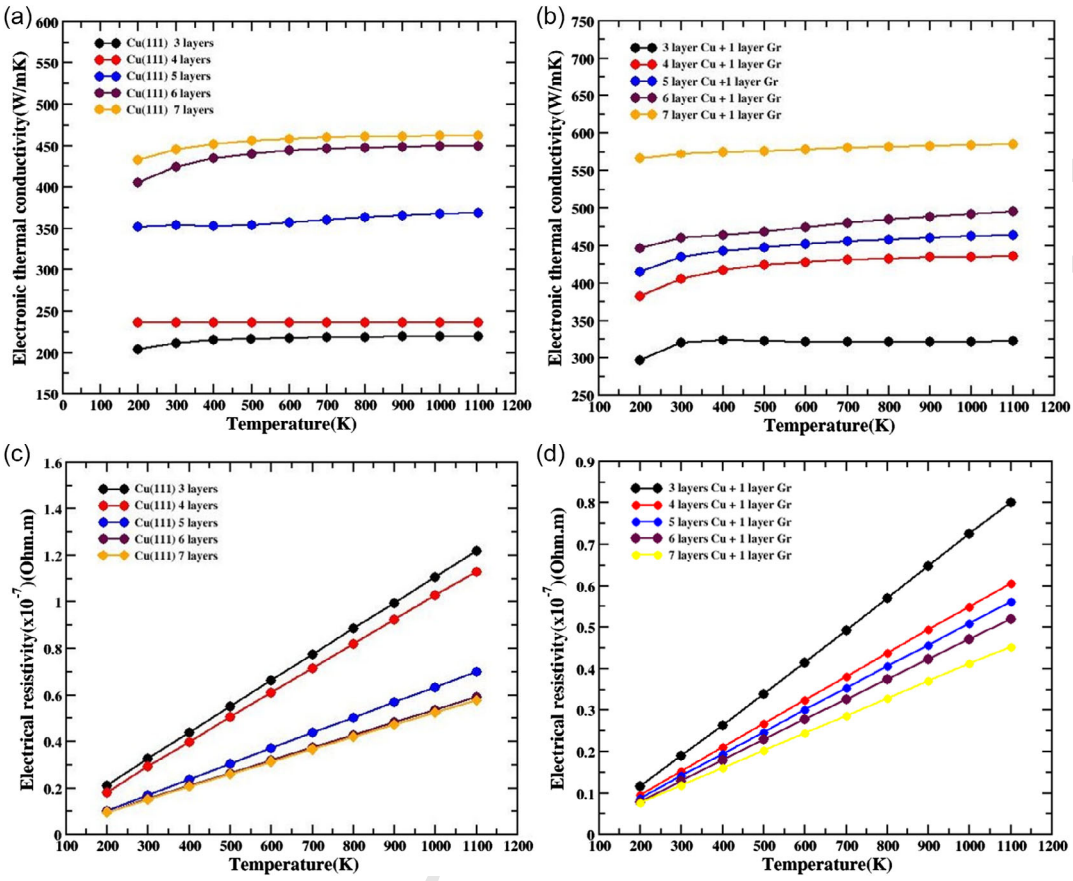

Q5 **Figure 4.** The variation of electronic thermal conductivity (κ_e) of a) Cu(111) surfaces and b) Cu(111)/SLG heterosystems by adding three to seven copper layers. The changes in electrical resistivity (ρ) of (a) Cu(111) surfaces and (b) Cu/SLG heterosystems by adding three to seven copper layers.

surface transport dominates and has a different character than bulk-like scattering (it is more resistive). As the thickness grows, bulk-like transport becomes more dominant, resulting in a lower resistivity/higher conductivity.

In Cu(111)/MLG heterosystem, seven layers of copper are used as a metal substrate for adding graphene layers. By adding three more graphene layers to the seven-layer Cu(111)/SLG heterosystem at room temperature, κ_e increases up to 148.37 W mK^{-1} (from 571.81 to 720.18 W mK^{-1}) and ρ decreases up to 0.035×10^{-7} Ωm (from 0.117×10^{-7} to 0.082×10^{-7} Ωm) for seven-layer Cu(111)/four-layer graphene, as shown in **Figure 5**a,b. Here, when a fourth graphene layer is added to the Cu(111)/MLG heterosystem, κ_e and ρ do not change significantly. The phonons increase as the temperature rises, enhancing the el-ph interaction. From Debye temperature onward, the number of phonons increases while the mean-free path of electrons decreases. As a result, κ_e does not change at high temperatures, as shown in Figure 4a,b and **5**b. Since ρ increases with rising temperature, σ decreases with temperature, as observed in Figure 4c,d as well as Figure 5b. An experimental observation shows a similar result, where TC enhances from copper/SLG to copper/MLG composites.[17] More specifically, Wejrzanowski et al.[17] conducted an experiment to investigate the effect of graphene thickness on the TC of a copper-graphene composite. They have applied two experimental techniques to develop Cu/Gr composites. In the first, graphene (SLG) was deposited on the copper foil (of a thickness of 35 μm) through chemical vapor deposition (CVD). In the second, a powder metallurgy technique is used to create mixtures of copper and multilayer graphene (MLG) powders. They found an increase in the volume fraction of MLG after depositing 10 layers of graphene on the copper film. By increasing the volume fraction of MLG, the TC of copper-MLG increases from 50 to 350 W mK^{-1}. Thus, our theoretical study is supported by an experiment where the in-plane TC of copper/graphene composites is enhanced by increasing the thickness of the graphene.[17] Apart from the experimental study, the lamellar model also supports our finding that the TC of the copper/MLG composite increases with increasing weight percentage and volume fraction of MLG.[17] Nath et al.[28] have reported that the TC and EC of thin films reduce with decreasing film thickness as per the Wiedemann–Franz law.[31] The variation of TC and EC with the thickness of Cu(111) primarily depends on two factors: 1) scattering of electrons; and 2) frozen-in structural defects. Further, the mean free path of electrons (the carriers of TC) is high at lower temperatures compared to higher temperatures.

To understand the interfacial properties of Cu(111)/Gr heterostructure, we have studied electronic band structure and density

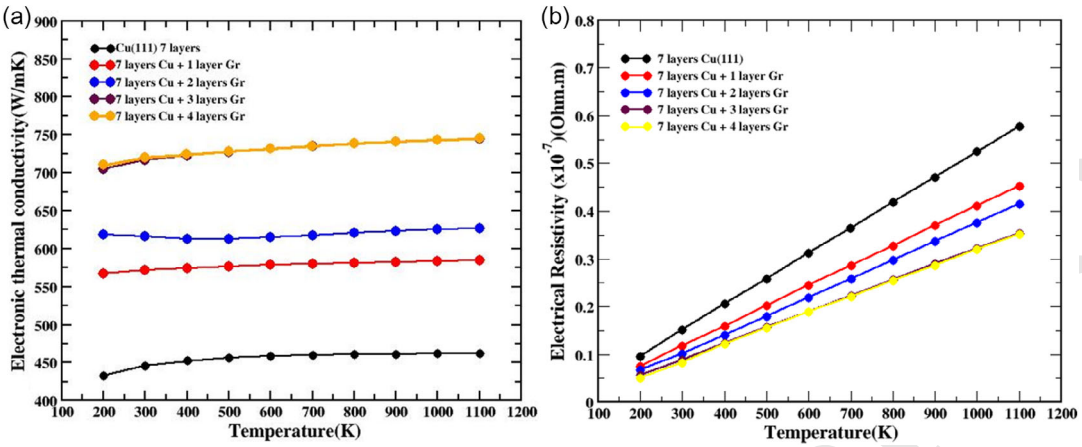

Figure 5. The variation of a) electronic thermal conductivity (κ_e) and b) electrical resistivity (ρ) of seven-layer Cu(111)/MLG heterosystems by adding one to four graphene layers.

of states (DOS). **Figure 6**a shows that few bands are crossing the Fermi level (set at energy 0.0 eV), and comparatively larger bands are available below the Fermi level. The DOS of the Cu(111)/Gr heterostructure is nonzero at the Fermi level. It should be noted that the DOS of graphene vanishes at Fermi level.[54,55] Thus, the DOS of the Cu/Gr heterostructure shows a drastic change compared to the pristine graphene. This interface allows a charge transfer between surfaces of Cu(111) and graphene. With increasing copper layers, the charge carriers are enhanced, which improves the EC and TC. Furthermore, as shown in Figure 6b, the work function difference between the SLG and copper layer allows for charge transfer from Cu(111) to the graphene surface. The band structure of the Cu(111)/graphene heterosystem also shows a shift in Fermi level from the Dirac cone point due to charge transfer to graphene from the Cu(111) surface.

The charge density difference ($\Delta\rho(r) = \rho_{\text{total}}(r) - \rho_{\text{Cu(111)}}(r) - \rho_{\text{graphene}}(r)$) is the difference between the total charge density of the Cu(111)/graphene heterosystem and individual charge densities (copper and graphene surfaces). The numerical value of the charge difference has been analyzed in terms of Bader charge analysis (**Table 1**). In a unit cell of the Cu(111)/graphene heterosystem, only three copper atoms and two carbon atoms are present. The $\Delta\rho(r)$ of terminating copper atoms and two carbon atoms (C1 and C2) are listed in Table 1. The $\Delta\rho(r)$ values show that charges are transferring from the copper atoms (of Cu(111)) to carbon atoms (of graphene) through the formation of a junction. A direct proportional relation has been observed between binding energy (BE) and charge transfer, as shown in Table 1. BE and $\Delta\rho(r)$ are much lower in the five-layer Cu(111)/SLG heterosystem than in other heterosystems. This is observed because Cu(111) binds with graphene in a B-type arrangement (i.e., the carbon atoms are not directly above the copper atoms and they are vertically above the hexagonal center of the copper arrangement), as shown in Figure S11 (Supporting Information). In a B-type arrangement, copper atoms are loosely bound with carbon atoms in graphene. In the A-type arrangement (i.e., the carbon

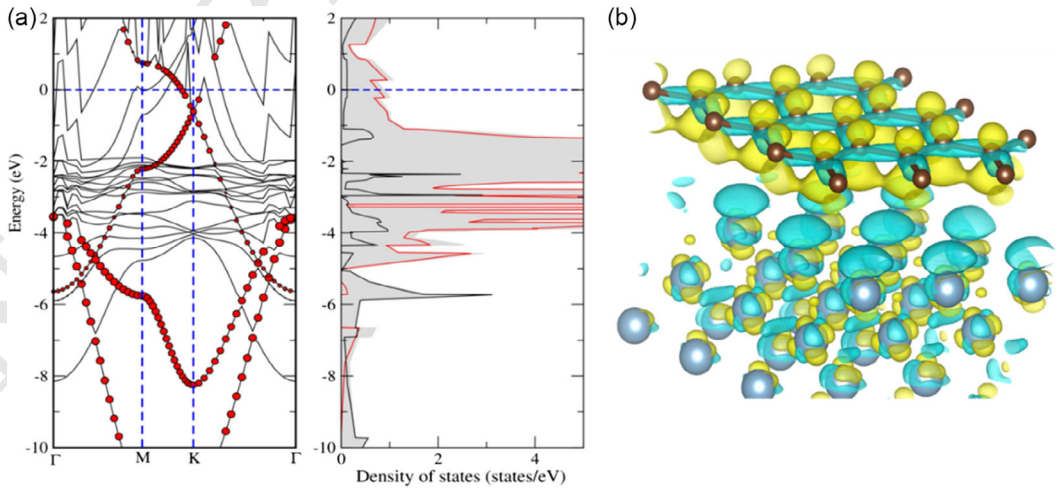

Figure 6. a) Band structure and density of states (DOS) of three-layer Cu(111)/SLG heterostructure. The contribution of the p_z-orbital of graphene is represented by the intensity of the red color in the band structure. b) Three-dimensional charge density plot of three-layer Cu(111)/SLG heterostructure. The yellow and cyan colors represent electron accumulation and depletion regions, respectively.

Table 1. Cu(111)/SLG heterosystem's binding energy (between copper and graphene surfaces), formation energy/atom, and charge difference with increasing copper thickness (from three to seven layers). Furthermore, the aforementioned parameters for the seven-layer Cu(111)/MLG heterosystem with increasing graphene thickness (from one to four layers).

Increasing copper layers (from three to seven) to Cu(111)/SLG heterosystems				
Heterosystems	Weight percentage	Binding energy [meV]	Formation energy/atom [meV]	Charge difference ($\Delta\rho$)
3-layer Cu(111)/SLG	Copper (88.80%), Graphene (11.20%)	−194.14	−38.82	C1 = 0.029
				C2 = 0.015
				Cu = −0.047
4-layer Cu(111)/SLG	Copper (91.36%), Graphene (8.64%)	−201.15	−33.52	C1 = 0.014
				C2 = 0.036
				Cu = −0.051
5-layer Cu(111)/SLG	Copper (92.97%), Graphene (7.02%)	−165.86	−23.69	C1 = 0.009
				C2 = 0.011
				Cu = −0.020
6-layer Cu(111)/SLG	Copper (94.07%), Graphene (5.93%)	−197.36	−24.67	C1 = 0.034
				C2 = 0.015
				Cu = −0.048
7-layer Cu(111)/SLG	Copper (94.88%), Graphene (5.12%)	−195.51	−21.72	C1 = 0.005
				C2 = 0.032
				Cu = −0.035
Increasing graphene layers (one to four) to seven-layer Cu(111)/MLG heterosystems				
7-layer Cu(111)/1-layer-graphene	Copper (94.88%), Graphene (5.12%)	−195.51	−21.72	C1 = 0.005
				C2 = 0.032
				Cu = −0.035
7-layer Cu(111)/2-layer-graphene	Copper (90.25%), Graphene (9.75%)	−221.96	−20.17	C1 = −0.002
				C2 = 0.022
				Cu = −0.039
7-layer Cu(111)/3-layer-graphene	Copper (86.06%), Graphene (13.94%)	−226.23	−17.40	C1 = 0.011
				C2 = 0.027
				Cu = −0.045
7-layer Cu(111)/4-layer graphene	Copper (82.25%), Graphene (17.75%)	−217.47	−14.50	C1 = 0.008
				C2 = 0.014
				Cu = −0.026

atoms are just above the copper atoms), copper atoms form a stronger bond. For interaction between Cu(111) and graphene surfaces, two of the three layers are A-type, while one is B-type. As a result, graphene creates a stronger binding in the ⅔ case compared to the other ⅓ case.

We also observed that with increasing thickness of graphene (from one to four layers) in the Cu(111)/MLG heterosystem, the BE (between copper and graphene) increases while the formation energy/atom decreases. With increasing copper thickness in the Cu(111)/SLG heterosystem, the weight percentage of copper increases from 88.80% (three-layer Cu(111)/SLG) to 94.88% (seven-layer Cu(111)/SLG), as shown in Table 1. For a fixed copper thickness (seven-layer Cu(111)/SLG), the weight percentage of graphene increases from 5.12% (for SLG) to 17.75% (for four-layer graphene). This implies that while BE (between copper and graphene) increases with increasing graphene weight percentage, it is less likely to form a large number of graphene layers on the Cu(111) substrate due to decreasing formation energy.

To further probe the interaction of Cu(111) and graphene surfaces, we have studied atomic orbital contribution through the projected density of states (PDOS), as shown in **Figure 7**. At the Fermi level, the p_z-orbital of the carbon atom (of graphene) directly interacts with the 3*d*-orbitals of copper (of Cu(111)), resulting in a nonzero state. These states are broadened further by increasing the number of copper and graphene layers in the Cu(111)/Gr heterostructure. As a result, the number of conduction electrons increases, which enhances the EC and TC. The electron localization function (ELF)[56] mapping is shown in **Figure 8**. The ELF values range from 0 to 1.0, indicating the order of localization of electrons in the position space. The ELF values at the copper and carbon atoms are 0.0 and 0.6, respectively. This is because valence electrons in a metallic copper atom are free, whereas they are highly localized in a

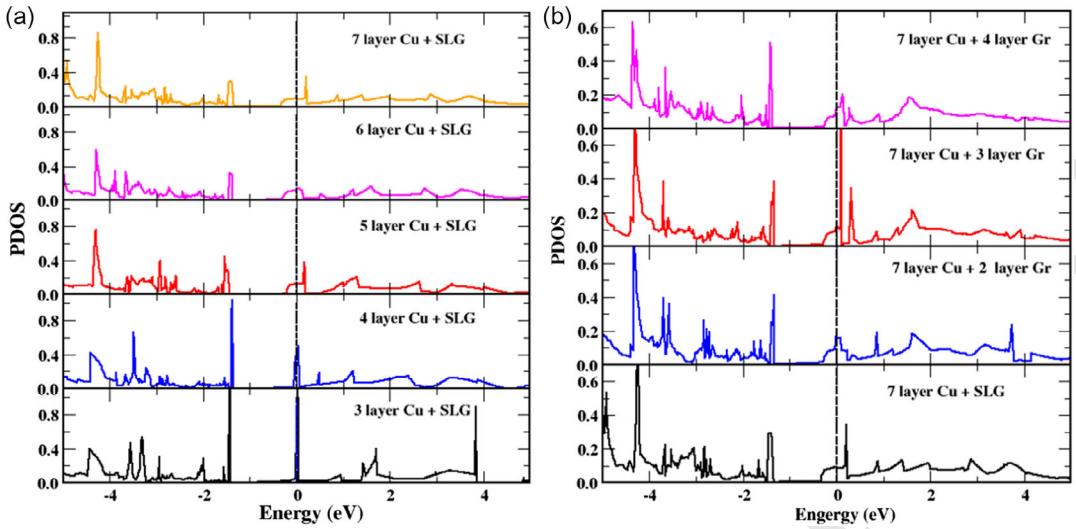

Figure 7. The projected density of states (PDOS) of the 2*p*-orbital of the carbon atom (of the graphene surface) is plotted for a) Cu(111)/SLG heterosystems with increasing copper layers (three to seven), and b) seven-layer Cu(111)/MLG heterosystems with increasing graphene layers (one to four).

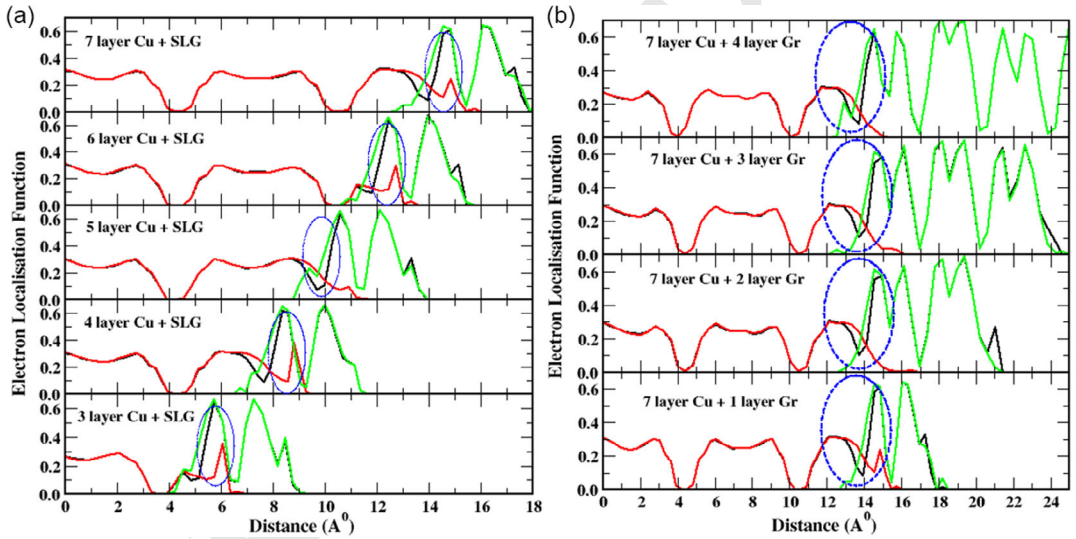

Figure 8. The electron localization functions (ELF) of a) Cu(111)/SLG heterosystems with increasing copper layers (three to seven) and b) seven-layer Cu(111)/MLG heterosystems with increasing graphene layers (one to four). The blue circles represent the junction of the copper and graphene surfaces.

nonmetallic carbon atom. A stronger localization has been found in the range 2.2–2.5 between copper atoms, which is due to metallic bonding.[57] The ELF values between 0.10 and 0.15 at Cu(111)/graphene junctions indicate the van der Waal interaction. The ELF of the Cu(111)/Gr heterosystem (Figure 8) shows that ELF decreases at the copper-graphene junction in both Cu(111)/SLG and Cu(111)/MLG heterosystems (Figure 8a,b. This means that at junctions, electrons are delocalized, resulting in an increased number of free electrons. A large number of free electrons enhance the EC and TC. Therefore, with increasing thickness of copper in the Cu(111)/SLG heterosystem, the κ_e increases up to 78% and the ρ decreases up to 33%. Furthermore, by increasing the thickness of graphene in a seven-layer Cu(111)/MLG heterosystem, the κ_e increases up to 26% while ρ decreases up to 30%.

4. Conclusions

In this work, we have studied the effect of strain (both tensile and compressive) and thickness on the transport properties (i.e., thermal conductivity (κ) and electrical conductivity (σ)) of the Cu(111)/graphene heterosystem through DFT. The conductivity contributed by electron and phonon is represented with electronic (κ_e) and phonon (κ_p) thermal conductivities, respectively. First, we applied tensile and compressive strain to the bulk copper, Cu(111) surface, and the Cu(111)/graphene heterosystem. The $\kappa_e(=520.247\,\mathrm{W\,mK^{-1}})$ plays the dominant role in TC over the $\kappa_p(=10.902\,\mathrm{W\,mK^{-1}})$ for bulk copper; therefore, the phonon transport part is ignored due to its very small contribution. The compressive strain on bulk copper and Cu(111) surfaces enhances the κ_e and σ. Both are reduced with a change in the

nature of strain, i.e., from compressive to tensile. The 0.20% compressive strain applied on the Cu(111)/graphene heterosystem increases κ_e and σ by up to 171% and 335%, respectively. We also found that compressive strain decreased the electron–phonon (el-ph) coupling, which increased κ_e and σ of the Cu(111)/graphene heterosystem.

We also found that increasing the thickness of copper and graphene (in terms of layers) in Cu(111)/SLG and Cu(111)/MLG heterosystems increases the values of κ_e and σ. With adding the copper layers (from three to seven) in the Cu(111)/SLG heterosystem, the κ_e increases up to 251.09 W mK^{-1} (from 320.72 to 571.81 W mK^{-1}) and ρ decreases up to $0.072 \times 10^{-7}\,\Omega$m (from 0.189×10^{-7} to $0.117 \times 10^{-7}\,\Omega$m). Adding more graphene layers (from one to four) in the seven-layer Cu(111)/MLG surface, κ_e increases up to 148.37 W mK^{-1} (from 571.81 to 720.18 W mK^{-1}) while ρ decreases up to $0.035 \times 10^{-7}\,\Omega$m (from 0.117×10^{-7} to $0.082 \times 10^{-7}\,\Omega$m). The origin of these changes in κ_e and σ has been probed by investigating bandstructure, DOS, charge transfer, and ELF. Lager available states near the Fermi level for Cu(111)/graphene heterostructures compared to graphene offer a large number of electrons for conduction from the valence bands to the conduction bands. The broadening of states at the Fermi energy level increases with increasing graphene and copper thickness in Cu(111)/graphene heterosystems. These states increase the number of conduction electrons, which enhance EC and TC. Furthermore, ELF analysis shows that electrons are delocalized at junctions, resulting in large free electrons that enhance EC and TC.

Supporting Information

Supporting Information is available from the Wiley Online Library or from the author.

Acknowledgements

The authors would like to acknowledge the funding agencies; MHRD Centre of Excellence for Novel Energy Material (CENEMA: RP-074), National Aluminium Company Limited (NALCO) consultancy project (RP274; entitled: Prototype Development, Fabrication and Validation of Al-Graphene Composites Battery with Cooling Plates). The simulations and/or computations were supported by the SAMKHYA: High-Performance Computing Facility provided by the Institute of Physics, Bhubaneswar and by National Param Supercomputing Facility (NPSF) provided by C-DAC Pune.

Conflict of Interest

The authors declare no conflict of interest.

Data Availability Statement

The data that support the findings of this study are available from the corresponding author upon reasonable request.

Keywords

copper/graphene heterosystem, density functional theory, electrical conductivity, strain, thermal conductivity

Received: August 18, 2022
Revised: March 17, 2023
Published online:

[1] A. A. Balandin, S. Ghosh, W. Bao, I. Calizo, D. Teweldebrhan, F. Miao, C. N. Lau, *Nano Lett.* **2008**, *8*, 902.
[2] A. K. Geim, K. S. Novoselov, in *Nanoscience and Technology: A Collection of Reviews from Nature Journals*, World Scientific **2010**, pp. 11–19. Q6
[3] R. F. Service, in *Carbon Sheets an Atom Thick Give Rise to Graphene Dreams*, American Association for the Advancement of Science **2009**.
[4] D. S. Ghosh, I. Calizo, D. Teweldebrhan, E. P. Pokatilov, D. L. Nika, A. A. Balandin, W. Bao, F. Miao, C. N. Lau, *Appl. Phys. Lett.* **2008**, *92*, 151911.
[5] Y. Gao, H. Wang, M. Sun, Y. Ding, L. Zhang, Q. Li, *Physica E* **2018**, *99*, 194.
[6] T. Y. Kim, C.-H. Park, N. Marzari, *Nano Lett.* **2016**, *16*, 2439.
[7] Y. Wang, Z. Lu, X. Ruan, *J. Appl. Phys.* **2016**, *119*, 225109.
[8] A. Jain, A. J. H. McGaughey, *Phys. Rev. B* **2016**, *93*, 81206.
[9] A. J. H. McGaughey, A. Jain, H.-Y. Kim, B. Fu, *J. Appl. Phys.* **2019**, *125*, 11101.
[10] Z. Tong, S. Li, X. Ruan, H. Bao, *Phys. Rev. B* **2019**, *100*, 144306.
[11] Q. Zhang, Y. Liu, T. Liao, C. Zhang, X. Wu, Y. Liu, M. S. Qurashi, F. Zheng, Q. Song, P. Han, *Mater. Chem. Phys.* **2019**, *231*, 188.
[12] Z. A. Ghaleb, M. Mariatti, Z. M. Ariff, *Composites, Part A* **2014**, *58*, 77.
[13] P. Goli, H. Ning, X. Li, C. Y. Lu, K. S. Novoselov, A. A. Balandin, *Nano Lett.* **2014**, *14*, 1497.
[14] H. Li, J. Sun, J. Zang, N. Su, X. Feng, Y. Shen, *Surf. Coat. Technol.* **2021**, *405*, 126554.
[15] S. Feng, Q. Guo, Z. Li, G. Fan, Z. Li, D.-B. Xiong, Y. Su, Z. Tan, J. Zhang, D. Zhang, *Acta Mater.* **2017**, *125*, 98.
[16] L. Wang, Z. Yang, Y. Cui, B. Wei, S. Xu, J. Sheng, M. Wang, Y. Zhu, W. Fei, *Sci. Rep.* **2017**, *7*. Q7
[17] T. Wejrzanowski, M. Grybczuk, M. Chmielewski, K. Pietrzak, K. J. Kurzydlowski, A. Strojny-Nedza, *Mater. Des.* **2016**, *99*, 163.
[18] R. Mehta, S. Chugh, Z. Chen, *Nano Lett.* **2015**, *15*, 2024.
[19] R. Mao, B. D. Kong, C. Gong, S. Xu, T. Jayasekera, K. Cho, K. W. Kim, *Phys. Rev. B* **2013**, *87*, 165410.
[20] K. Jagannadham, *J. Appl. Phys.* **2011**, *110*, 74901.
[21] I. Firkowska, A. Boden, B. Boerner, S. Reich, *Nano Lett.* **2015**, *15*, 4745.
[22] K. M. Mohsin, A. Srivastava, A. K. Sharma, C. Mayberry, M. S. Fahad, *ECS J. Solid State Sci. Technol.* **2017**, *6*, P119.
[23] N. Wei, L. Xu, H.-Q. Wang, J.-C. Zheng, *Nanotechnology* **2011**, *22*, 105705.
[24] F. Ma, H. B. Zheng, Y. J. Sun, D. Yang, K. W. Xu, P. K. Chu, *Appl. Phys. Lett.* **2012**, *101*, 111904.
[25] S. Bazrafshan, A. Rajabpour, *Int. J. Heat Mass Transfer* **2017**, *112*, 379.
[26] H.-F. Lee, S. Kumar, M. A. Haque, *Acta Mater.* **2010**, *58*, 6619.
[27] X. Li, K. Maute, M. L. Dunn, R. Yang, *Phys. Rev. B* **2010**, *81*, 245318.
[28] P. Nath, K. L. Chopra, *Thin Solid Films* **1974**, *20*, 53.
[29] M. R. Sahoo, S. Sahu, A. K. Kushwaha, S. K. Nayak, in *AIP Conf. Proceedings*, AIP Publishing LLC, **2018**, p. 90047.
[30] S. Sahu, M. R. Sahoo, A. K. Kushwaha, G. C. Rout, S. K. Nayak, *Carbon* **2019**, *142*, 685.
[31] N. Stojanovic, D. H. S. Maithripala, J. M. Berg, M. Holtz, *Phys. Rev. B* **2010**, *82*, 75418.
[32] S. Y. Savrasov, D. Y. Savrasov, *Phys. Rev. B* **1996**, *54*, 16487.
[33] P. E. Blochl, *Phys. Rev. B* **1994**, *50*, 17953.
[34] J. P. Perdew, K. Burke, M. Ernzerhof, *Phys. Rev. Lett.* **1996**, *77*, 3865.
[35] A. F. F. de F. Pereira, S. M. de Souza, A. Ghosh, *Mater. Today Commun.* **2020**, *25*, 101613.

[36] K. Mizokami, A. Togo, I. Tanaka, *Phys. Rev. B* **2018**, *97*, 224306.
[37] M. M. Dacorogna, M. L. Cohen, P. K. Lam, *Phys. Rev. Lett.* **1985**, *55*, 837.
[38] A. I. Liechtenstein, I. I. Mazin, C. O. Rodriguez, O. Jepsen, O. K. Andersen, M. Methfessel, *Phys. Rev. B* **1991**, *44*, 5388.
[39] A. Giri, J. T. Gaskins, L. Li, Y.-S. Wang, O. V. Prezhdo, P. E. Hopkins, *Phys. Rev. B* **2019**, *99*, 165139.
[40] M. Raeisi, S. Ahmadi, A. Rajabpour, *Nanoscale* **2019**, *11*, 21799.
[41] M. R. Sahoo, A. K. Kushwaha, R. Pati, P. M. Ajayan, S. K. Nayak, *J. Magn. Magn. Mater.* **2019**, *484*, 462.
[42] G. Giovannetti, P. A. Khomyakov, G. Brocks, V. M. Karpan, J. van den Brink, P. J. Kelly, *Phys. Rev. Lett.* **2008**, *101*, 26803.
[43] P. A. Khomyakov, G. Giovannetti, P. C. Rusu, G. Brocks, J. Van den Brink, P. J. Kelly, *Phys. Rev. B* **2009**, *79*, 195425.
[44] E. Khan, T. S. Rahman, S. Subrina, *J. Appl. Phys.* **2016**, *120*, 185101.
[45] W. Liu, Y. Yang, M. Asheghi, in *Thermal and Thermomechanical Proceedings 10th Intersociety Conf. on Phenomena in Electronics Systems, 2006. ITHERM 2006*, IEEE, Piscataway, NJ **2006**, pp. 1171–1176.
[46] L. Zheng, H. Zheng, D. Huo, F. Wu, L. Shao, P. Zheng, Y. Jiang, X. Zheng, X. Qiu, Y. Liu, *Sci. Rep.* **2018**, *8*.
[47] N. A. Lanzillo, J. B. Thomas, B. Watson, M. Washington, S. K. Nayak, *Proc. Natl. Acad. Sci.* **2014**, *111*, 8712.
[48] B. D. Kong, S. Paul, M. B. Nardelli, K. W. Kim, *Phys. Rev. B* **2009**, *80*, 33406.
[49] R. D'Souza, S. Mukherjee, *Phys. Rev. B* **2017**, *95*, 85435.
[50] C. Si, Z. Liu, W. Duan, F. Liu, *Phys. Rev. Lett.* **2013**, *111*, 196802.
[51] S. Chen, A. L. Moore, W. Cai, J. W. Suk, J. An, C. Mishra, C. Amos, C. W. Magnuson, J. Kang, L. Shi, *ACS Nano* **2011**, *5*, 321.
[52] J. H. Seol, I. Jo, A. L. Moore, L. Lindsay, Z. H. Aitken, M. T. Pettes, X. Li, Z. Yao, R. Huang, D. Broido, *Science* **2010**, *328*, 213.
[53] W. Cai, A. L. Moore, Y. Zhu, X. Li, S. Chen, L. Shi, R. S. Ruoff, *Nano Lett.* **2010**, *10*, 1645.
[54] D. Zhan, J. Yan, L. Lai, Z. Ni, L. Liu, Z. Shen, *Adv. Mater.* **2012**, *24*, 4055.
[55] A. Bostwick, J. McChesney, T. Ohta, E. Rotenberg, T. Seyller, K. Horn, *Prog. Surf. Sci.* **2009**, *84*, 380.
[56] A. D. Becke, K. E. Edgecombe, *J. Chem. Phys.* **1990**, *92*, 5397.
[57] K. Koumpouras, J. A. Larsson, *J. Phys.: Condens. Matter* **2020**, *32*, 315502.